PHYSICAL REVIEW A **95**, 051801(R) (2017)

Radial index of Laguerre-Gaussian modes in high-order-harmonic generation

Romain Géneaux,[1,*] Céline Chappuis,[1] Thierry Auguste,[1] Samuel Beaulieu,[2,3] Timothy T. Gorman,[4] Fabien Lepetit,[1] Louis F. DiMauro,[4] and Thierry Ruchon[1]

[1]*LIDYL, CEA, CNRS, Université Paris-Saclay, CEA Saclay, 91191 Gif-sur-Yvette, France*

[2]*Université de Bordeaux CNRS CEA, CELIA, UMR5107, F33405 Talence, France*

[3]*Institut National de la Recherche Scientifique, J3X 1S2 Varennes, Québec, Canada*

[4]*Department of Physics, The Ohio State University, Columbus, Ohio 43210, USA*

(Received 23 March 2017; published 16 May 2017)

High-order-harmonic generation (HHG) is a tabletop and tunable source of extreme ultraviolet (XUV) light. Its flexibility was lately evidenced by the production of Laguerre-Gaussian (LG) modes in the XUV with a known azimuthal index. Here we investigate the role of the radial index of LG modes in HHG. We show both numerically and experimentally that the mode content of the emitted XUV radiation can be tuned by controlling the weight of the different quantum trajectories involved in the process. The appearance of high-order radial modes is finally linked to the atomic dipole phase of HHG. These results extend the capabilities of shaping the spatial mode of ultrashort XUV pulses of light.

DOI: 10.1103/PhysRevA.95.051801

I. INTRODUCTION

In many areas of physics, intriguing and unexpected behaviors have been linked to the presence of topological singularities. Optics has its own singularities that occur whenever a quantity such as the phase or the polarization of the electromagnetic field cannot be defined [1]. A preeminent example of such field is that of the Laguerre-Gaussian modes, which possess a phase singularity in their center. They have been used in a plethora of different applications, mainly because they carry a well-defined orbital angular momentum (OAM) [2].

The Laguerre-Gaussian (LG) modes form a complete set of solutions to the paraxial wave equation, and are indexed by two mode numbers, denoted as ℓ and p, respectively called the azimuthal and radial indexes. These names stem from the fact that along the azimuthal coordinate θ, the phase of these modes goes as $\ell\theta$, while their radial profile shows $p+1$ concentric rings for $\ell > 0$.

Until recently, the production of LG modes was mastered only in the visible and infrared spectral range. Three separate works [3–5] recently demonstrated that this could be extended in the extreme ultraviolet (XUV) range using high-order-harmonic generation (HHG) in gases. By focusing an infrared laser in an atomic or molecular target, HHG is able to produce ultrashort pulses of XUV light made of many harmonics of the driving field. The aforementioned works showed that if the driver is a $(\ell_1,0)$ LG mode, each emitted high-order harmonic will be a LG mode as well. In particular, it was shown that the azimuthal index of the qth harmonic, ℓ_q, can be chosen to be unity if the generating medium is long [3], equal to $q \times \ell_1$ for thinner media [4,5], or tuned to some extent using two generating beams [6,7].

These results open up many possibilities of fundamental studies such as the exchange of OAM in light-matter interactions [8,9]. Moreover, they are an example of refined structuring of the light spatial mode in the XUV, a difficult but promising task [10,11].

Hitherto, none of these studies tackled the question of the radial index, p, of the generated modes. The situation was long similar in the visible range, where p has been dubbed the "forgotten quantum number," before its physical significance was more thoroughly investigated [12,13]. The radial index came to be used in quantum optics, where it enabled producing entangled states of impressively high dimension [14,15]. Even in less fundamental studies it has found several purposes; for instance, modes with high values of p revealed self-healing properties similar to Bessel beams [16], can overcome the diffraction limit when strongly focused [17], or turned out to be paramount when extreme interferometric stability is needed [18]. Controlling both the ℓ and p indices in HHG is thus an access road to a full shaping of XUV and ultrashort pulses.

In the present work, we study the role of the radial index in high-order-harmonic generation driven by a Laguerre Gaussian mode (LG-HHG). First, we perform a numerical simulation showing that it is possible to produce multiringed intensity patterns, characteristic of $p > 0$ modes, by controlling the weights of the quantum trajectories of HHG. We then conduct the experiment, which demonstrates the possibility of continuously going from a single- to a multiringed intensity pattern for the XUV radiation. Finally, we discuss the creation of these $p > 0$ modes in LG-HHG and track their appearance back to the atomic dipole phase of HHG.

II. NUMERICAL SIMULATION OF LG-HHG

To realistically describe HHG, the process has to be considered at the microscopic and macroscopic scale. At the single-atom level, the Lewenstein model [19] shows that two different quantum paths can be identified [20], the so-called "short" and "long" trajectories. At the macroscopic scale, the contribution of all atoms in the interaction region must be coherently summed and the resulting emission is governed by the phase-matching conditions. With an usual Gaussian driver, the short (respectively, long) trajectory is better phase matched if the focus of the generating laser is slightly before (respectively, after) the gas medium [20].

When the driving beam is given a Laguerre-Gaussian profile, the microscopic process is not expected to change, for

*romain.geneaux@cea.fr

if we stay well in the paraxial regime, the beam is still seen as a plane wave at the atomic scale. On the other hand, the transverse profile of a Laguerre-Gaussian mode will influence phase matching. This has been known for a long time for other kinds of non-Gaussian modes, such as truncated-Bessel modes [21,22]. Let us recall the expression of the electric field of the (ℓ,p) LG mode in the (r,θ,z) cylindrical coordinates, omitting the normalization constants:

$$E_{\ell,p}(r,\theta,z) = \frac{e^{i\ell\theta}}{w(z)}\left(\frac{r}{w(z)}\right)^{|\ell|} L_p^{|\ell|}\left(\frac{2r^2}{w^2(z)}\right) \times e^{\{-[r^2/w^2(z)]-ik[r^2/2R(z)]-ikz+i(2p+|\ell|+1)\chi(z)\}}, \quad (1)$$

where $w(z)$, $R(z)$, and $\chi(z)$ are, respectively, the beam waist, wave-front curvature, and Gouy phase, and $L_p^{|\ell|}$ are the generalized Laguerre polynomials, which are responsible for the multiringed patterns of $p > 0$ modes.

To understand the interplay between the quantum paths and the p mode content of HHG, we carry out a numerical simulation of LG-HHG taking into account all aspects of a real experiment, including the propagation of the infrared beam toward and inside the gas target. We consider an incident Gaussian laser beam of 6.25 mm waist and 50 fs duration, numerically propagated through a spiral phase plate, which adds the $e^{i\theta}$ transverse phase of the (1,0) LG mode [23]. It is then focused by a 1 m focal length lens in a 500-μm−wide Lorentzian argon gas jet, where high-order harmonics are emitted. The details of the model, which accounts for the full three-dimensional propagation of the beam including dispersion, can be found in Ref. [5]. The calculation is repeated for three different values of z_0, the position of the laser focus compared to the center of the generating medium. The intensity profiles obtained in the far field are displayed in Fig. 1.

When $z_0 < 0$, the intensity pattern shows a single ring, reminiscent of a $p = 0$ mode. On the contrary, the profile for $z_0 > 0$ is multiringed. It seems richer in the intermediate $z_0 = 0$ case. These patterns can be deciphered by looking at the two trajectories separately, which is done by choosing one solution of the saddle-point equations. This yields the profiles presented in the bottom row of Fig. 1. This shows that the short (respectively, long) trajectory contribution shows one (respectively, several) ring(s). Interestingly, phase matching does not appear to be drastically modified by the infrared LG mode, for the selection of one quantum trajectory follows the same behavior as in the Gaussian case. Nevertheless, it is probable that the LG mode modifies finer details of phase matching—such as efficiency as a function of various generation parameters—similarly to what is observed in the visible range [24], but this goes beyond the scope of our study. Finally, the intricate profile of the intermediate $z_0 = 0$ case appears as the result of quantum path interference, an effect well known in HHG driven by Gaussian beams [25].

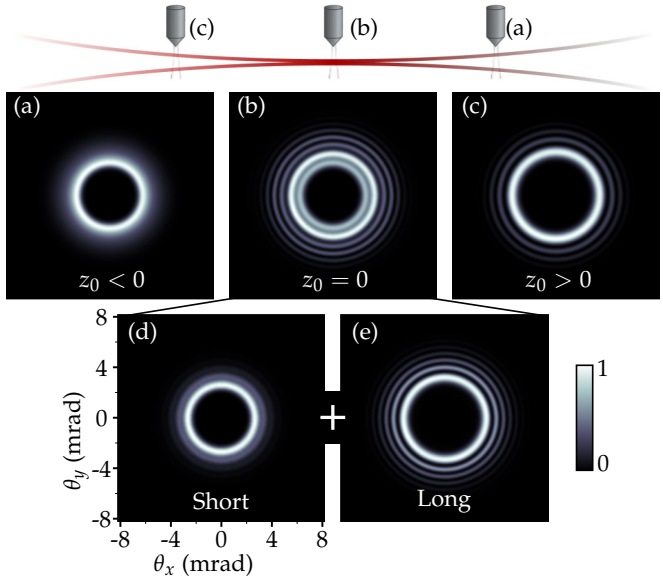

FIG. 1. Contributions of different quantum trajectories in LG-HHG. The intensity of the 21st harmonic in argon is computed in the far field for (a) $z_0 < 0$, (b) $z_0 = 0$, and (c) $z_0 > 0$, where z_0 is the position of the laser focus compared to the gas jet. (d) and (e) show the profile in $z_0 = 0$ when only the short or long trajectory contribution is selected.

III. EXPERIMENT

A. Setup

We now set to measuring the multi-ringed patterns of Fig. 1 experimentally. The experiments were done using the LUCA laser server at CEA Saclay, which delivers 30 mJ, 50 fs, 800 nm pulses at 20 Hz. In this rather typical Ti:sapphire laser chain, a hollow core fiber is added right before the compressor, which filters the laser spatial profile and guarantees an almost perfect Gaussian mode [26]. This mode is then converted using a 16-level spiral phase plate (SPP) (SILIOS Technologies), which yields a 77.5% pure (1,0) Laguerre-Gaussian mode [27]. A 1 m lens (L) focuses the beam into an argon gas jet provided by a piezoelectric-driven valve (Attotech).

The numerical results presented above show that we need to spectrally separate and measure the two-dimensional (2D) spatial transverse profile of the emitted harmonics. To disperse the different harmonics, typical HHG setups use cylindrical gratings which focus each spectral component in one dimension, eventually yielding a spatiospectral measurement. Clearly, such gratings cannot be employed to image the patterns of Fig. 1. To solve this issue, we opt for a simple and cost-effective design initially proposed in Ref. [28]. Since the spectral resolution needs only to be good enough for the harmonics not to overlap, we use a flat grating of which only a few grooves are illuminated. The complete setup implementing this idea is sketched in Fig. 2(a). First, the harmonic radiation is reimaged by a toroidal mirror (TM) coupled with a silica plate (SP), which filters most of the remaining generation beam. The beam is then reflected off a spherical mirror at a 10° incidence angle. This mirror is treated with a B_4C coating (Fraunhofer Institute), which has a reflectivity higher than 10% in the 30–800 nm spectral range. Close to the focus of this mirror, the beam strikes a flat diffraction grating (600 grooves/mm, Spectrogon) at 6° incidence. The beam therefore illuminates about 200 grooves, reducing dispersion and inducing close to no distortion on

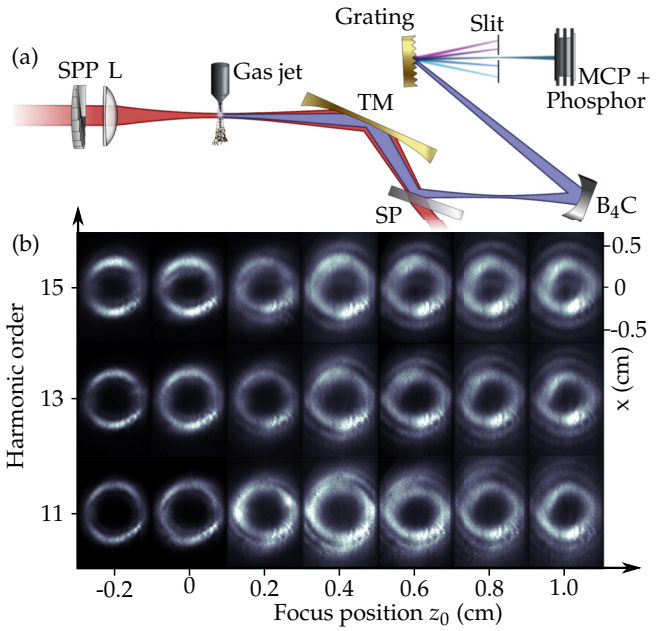

FIG. 2. Measurement of the harmonic intensity profile as a function of the focus position. (a) Experimental setup for LG-HHG and measurement of the 2D spatial profile of several harmonics. The acronyms used for the optical elements are defined in the text. (b) Intensity profiles of harmonics 11–15 when the generating lens is translated over 1.2 cm. The intensity of each harmonic is normalized to 1. $z = 0$ is known from previous experiments done with Gaussian drivers on this beamline.

the harmonic profiles. The harmonics are finally selected by a slit before being imaged by microchannel plates (MCPs) coupled to a phosphor screen, imaged by a 12-bit CCD camera (Basler). This design does not use any sophisticated optics, resulting in an extremely low cost compared to typical spectrometers used in HHG while minimizing spatiospectral couplings.

B. Results

Just as we did numerically, the relative weights of the quantum trajectories are controlled by varying z_0, which in practice is simply the position of the lens. Figure 2(b) shows the evolution of the intensity profiles of harmonics 11–15 when z_0 is changed over 1.2 cm.

We observe a series of cylindrically symmetric rings, evidence that we indeed measure the spatiospatial harmonic profiles and not a spatiospectral convolution. For $z_0 = -0.2$ cm, the harmonics show only one ring, reminiscent of the short trajectory contribution in Fig. 1. At $z_0 = 0$, an additional ring appears inside the former, which can be interpreted as quantum path interferences following the prediction of Fig. 1(b). Then, more divergent concentric rings keep appearing as z_0 is increased. As explained above, these rings are due to the long trajectory of HHG and suggest the generation of $p > 0$ Laguerre-Gaussian modes. To further strengthen this claim, in the following part, we turn to numerical calculations to track how additional $p > 0$ modes could be created in LG-HHG.

IV. MODAL ANALYSIS OF LG-HHG

As shown in Refs. [13,29], p is a quantum number associated to an operator acting on the light field, the expression of which is also given in those references. These works show that just as linear momentum is related to translation, or angular momentum to rotation, p is related to the dilatation along the radial coordinate. Therefore, just as any external torque modifies the angular momentum of a system, any effect affecting the radial dilatation of the beam will modify the p mode content of the light field. Two such effects can be identified in HHG:

(1) The nonlinearity of HHG: if a process has an order of nonlinearity n, the emitted field goes as $E_{\text{out}} = E_{\text{in}}^n$. Using Eq. (1) we see that if E_{in} is a LG mode with $p > 0$, E_{out} is not a pure LG mode.

(2) The atomic dipole phase: the spatial phase of the harmonic field varies linearly with the infrared intensity I_{IR}. It can be written as $\phi_{\text{at}}(r,\theta) = \alpha_{\text{traj}} I_{\text{IR}}(r,\theta)$, where α_{traj} is a constant which depends on the quantum trajectory [20]. Here, $\phi_{\text{at}}(r,\theta)$ will be ring shaped, following the intensity of the driving Laguerre-Gaussian mode.

To study these effects, we adopt a simpler description of HHG, which will allow us to repeat the calculation for a large number of parameters. From now on we neglect all effects due to neutral and plasma dispersion, propagation, and depletion in the gas jet. The gas medium is considered as an infinitely thin atomic plane, where HHG occurs. This approach neglects longitudinal effects and was used in Refs. [30,31]. It is valid as long as we stay away from larger interaction volumes such as the case of Ref. [3].

First, the infrared field is numerically propagated through the SPP and then toward the focus, where it reaches a peak intensity of 1.2×10^{14} W/cm. From this intensity, the ionization rate is computed using the Ammosov-Delone-Krainov formula [32] and the harmonic field is obtained in the strong-field approximation [19]. It is then propagated in the far field and decomposed onto the Laguerre-Gaussian basis. The complex coefficients of this decomposition, denoted as $c_{\ell,p}$, give the contribution of the (ℓ, p) LG mode. In Fig. 3, we show separately the result for the two quantum trajectories in the case of the 19th harmonic. Remarkably, we see that the (19,0) mode accounts for 98.9% of the short trajectory contribution: the harmonic field is even purer than the driving field itself. This is a result of the high nonlinearity of the process, in which the fainter rings of the $p > 0$ modes constituting the infrared field do not contribute. We can therefore rule out effect (1) as the source of additional p modes.

The long trajectory contribution behaves differently. Its modal decomposition shows that the (19,0) mode only constitutes 52% of the total emission, which is actually made of a large number of modes with p ranging from 0 to $\simeq 30$. The relative phase of these modes is such that their interference leads to a single ring at focus, but since they have different Gouy phases [see Eq. (1)], the relative phases vary until the distance of propagation reaches the Rayleigh range. As a result, the intensity of the emission shows a multiringed pattern in the

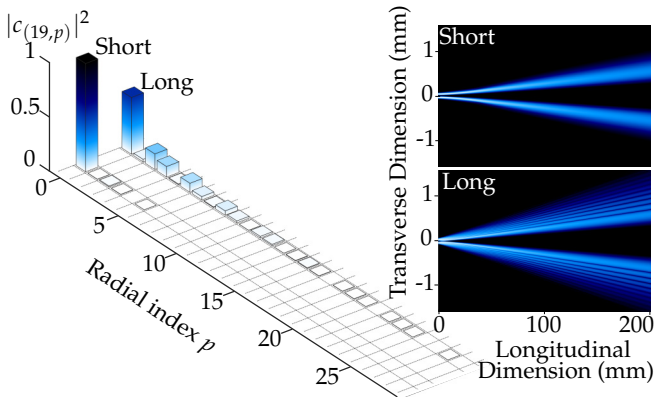

FIG. 3. Modal analysis of quantum trajectories. Left: Coefficients of the decomposition of the electric field of harmonic 19 onto the Laguerre-Gaussian basis for the short and long trajectories. Coefficients for other values of ℓ_{19} are null. Right: Intensity of harmonic 19 for the short and long trajectories upon numerical propagation over 200 mm.

far field, as evidenced in the right panel of Fig. 3. This contrast with the short trajectory can be explained by the atomic dipole phase, which is much stronger for the long quantum path: the proportionality coefficient is typically $\alpha_{\text{long}} \sim -20 \times 10^{-14}$ cm/W, while $\alpha_{\text{short}} \sim -1 \times 10^{-14}$ cm/W. We can therefore conclude that the atomic dipole phase ϕ_{at} allows for a control of the p mode content of the emission, by tuning the weight of the quantum paths.

Finally, since ϕ_{at} can be written as $\phi_{\text{at}}(r,\theta) = \alpha_{\text{traj}} I_{\text{IR}}(r,\theta)$, it should also be possible to tune the p mode content by controlling the intensity of the infrared field. We repeat the previous calculation when the peak infrared intensity varies from 1 to 2.4×10^{14} W/cm. Figure 4 shows the $(\ell = 19, p)$ mode decomposition for each intensity value and each trajectory. We see that even at high intensities, the short trajectory contribution is always strongly dominated by the (19,0) mode. On the other hand, the number of p modes of the long trajectory can be continuously increased by raising the infrared intensity. Another observation is that although modes with high values of p contribute to the emission, it is nowhere close to a pure (ℓ, p) LG mode. If XUV high-order vortices with high purity are required, other schemes of generation will be needed. For instance, driving HHG directly with a $p > 0$ infrared beam might lead to interesting mode contents in the XUV, although we have seen that outer rings tend to contribute less due to the nonlinearity of HHG.

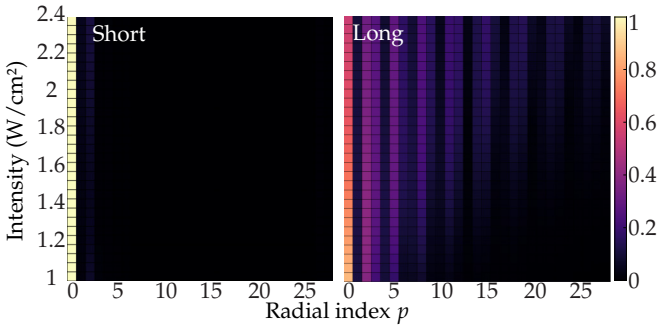

FIG. 4. Mode content as a function of the driving intensity. Coefficients of the decomposition of harmonic 19 when the infrared peak intensity is varied from to 1 to 2.4×10^{14} W/cm.

V. CONCLUSION

In conclusion, we have demonstrated the link between the quantum paths of HHG and the radial index of the emitted extreme ultraviolet vortices. We demonstrated both theoretically and experimentally that controlling the weight of these quantum trajectories produced very different intensity patterns for the harmonic emission. These patterns were then explained by the creation of new p modes by the atomic dipole phase, a well-known quantity in conventional HHG. First, our work demonstrates that previous experiments of LG-HHG in similar conditions [4,5] measured highly pure $(\ell_q,0)$ LG modes and not a superposition of several modes of various radial indexes. Second, we extended these experiments and showed the generation of LG modes in the extreme ultraviolet, this time with high p values. Additionally to this short wavelength, the emitted radiation shows a rich attosecond time structure, as theoretically investigated in Ref. [33]. The control of this additional quantum number in this attractive spectral and temporal range is a step toward tailoring more complex and refined XUV light sources for fundamental studies and applications.

ACKNOWLEDGMENTS

We thank A. Camper and Y. Mairesse for fruitful discussion and useful comments on the manuscript. We acknowledge financial support of the French National Research Agency (ANR), through XSTASE (ANR-14-CE32-0010). S.B. acknowledges support from the Vanier Scholarship program. Work by T.T.G. and L.F.D. was supported by the U.S. Department of Energy (DOE), Office of Science, Basic Energy Sciences (BES) under Grants No. DE-SC0012462 and No. DE-FG02-04ER15614, respectively.

[1] J. Nye and M. Berry, Dislocations in wave trains, Proc. R. Soc. London, Ser. A **336**, 165 (1974).

[2] L. Allen, M. W. Beijersbergen, R. J. C. Spreeuw, and J. P. Woerdman, Orbital angular momentum of light and the transformation of laguerre-gaussian laser modes, Phys. Rev. A **45**, 8185 (1992).

[3] M. Zürch, C. Kern, P. Hansinger, A. Dreischuh, and C. Spielmann, Strong-field physics with singular light beams, Nat. Phys. **8**, 743 (2012).

[4] G. Gariepy, J. Leach, K. T. Kim, T. J. Hammond, E. Frumker, R. W. Boyd, and P. B. Corkum, Creating High-Harmonic Beams with Controlled Orbital Angular Momentum, Phys. Rev. Lett. **113**, 153901 (2014).

[5] R. Géneaux, A. Camper, T. Auguste, O. Gobert, J. Caillat, R. Taïb, and T. Ruchon, Synthesis and characterization of attosecond light vortices in the extreme ultraviolet, Nat. Commun. **7**, 12583 (2016).

[6] D. Gauthier, P. Rebernik Ribič, G. Adhikary, A. Camper, C. Chappuis, R. Cucini, L. F. DiMauro, G. Dovillaire, F. Frassetto, R. Géneaux, P. Miotti, L. Poletto, B. Ressel, C. Spezzani, M. Stupar, T. Ruchon, and G. De Ninno, Tunable orbital angular momentum in high-harmonic generation, Nat. Commun. **8**, 14971 (2017).

[7] F. Kong, C. Zhang, F. Bouchard, Z. Li, G. G. Brown, D. H. Ko, T. J. Hammond, L. Arissian, R. W. Boyd, E. Karimi, and P. B. Corkum, Controlling the orbital angular momentum of high harmonic vortices, Nat. Commun. **8**, 14970 (2017).

[8] M. Babiker, C. R. Bennett, D. L. Andrews, and L. C. Dávila Romero, Orbital Angular Momentum Exchange in the Interaction of Twisted Light with Molecules, Phys. Rev. Lett. **89**, 143601 (2002).

[9] M. van Veenendaal and I. McNulty, Prediction of Strong Dichroism Induced by X Rays Carrying Orbital Momentum, Phys. Rev. Lett. **98**, 157401 (2007).

[10] A. Camper, T. Ruchon, D. Gauthier, O. Gobert, P. Salières, B. Carré, and T. Auguste, High-harmonic phase spectroscopy using a binary diffractive optical element, Phys. Rev. A **89**, 043843 (2014).

[11] G. Pariente and F. Quéré, Spatio-temporal light springs: Extended encoding of orbital angular momentum in ultrashort pulses, Opt. Lett. **40**, 2037 (2015).

[12] E. Karimi, R. W. Boyd, P. de la Hoz, H. de Guise, J. Řeháček, Z. Hradil, A. Aiello, G. Leuchs, and L. L. Sánchez-Soto, Radial quantum number of laguerre-gauss modes, Phys. Rev. A **89**, 063813 (2014).

[13] W. N. Plick and M. Krenn, Physical meaning of the radial index of laguerre-gauss beams, Phys. Rev. A **92**, 063841 (2015).

[14] V. D. Salakhutdinov, E. R. Eliel, and W. Löffler, Fullfield Quantum Correlations of Spatially Entangled Photons, Phys. Rev. Lett. **108**, 173604 (2012).

[15] M. Krenn, M. Huber, R. Fickler, R. Lapkiewicz, S. Ramelow, and A. Zeilinger, Generation and confirmation of a (100×100)-dimensional entangled quantum system, Proc. Natl. Acad. Sci. USA **111**, 6243 (2014).

[16] J. Mendoza-Hernández, M. L. Arroyo-Carrasco, M. D. Iturbe-Castillo, and S. Chávez-Cerda, Laguerre-gauss beams versus bessel beams showdown: Peer comparison, Opt. Lett. **40**, 3739 (2015).

[17] D. A. Savelyev, S. N. Khonina, and I. Golub, Tight focusing of higher orders laguerre-gaussian modes, AIP Conf. Proc. **1724**, 020021 (2016).

[18] M. Granata, C. Buy, R. Ward, and M. Barsuglia, Higher-Order Laguerre-Gauss Mode Generation and Interferometry for Gravitational Wave Detectors, Phys. Rev. Lett. **105**, 231102 (2010).

[19] M. Lewenstein, P. Balcou, M. Y. Ivanov, A. L'Huillier, and P. B. Corkum, Theory of high-order harmonic generation by low-frequency laser fields, Phys. Rev. A **49**, 2117 (1994).

[20] P. Salières, A. L'Huillier, and M. Lewenstein, Coherence Control of High-Order Harmonics, Phys. Rev. Lett. **74**, 3776 (1995).

[21] M. Nisoli, E. Priori, G. Sansone, S. Stagira, G. Cerullo, S. De Silvestri, C. Altucci, R. Bruzzese, C. De Lisio, P. Villoresi *et al.*, High-Brightness High-Order Harmonic Generation by Truncated Bessel Beams in the Sub-10-fs Regime, Phys. Rev. Lett. **88**, 033902 (2002).

[22] C. Altucci, R. Bruzzese, C. De Lisio, M. Nisoli, E. Priori, S. Stagira, M. Pascolini, L. Poletto, P. Villoresi, V. Tosa *et al.*, Phase-matching analysis of high-order harmonics generated by truncated bessel beams in the sub-10-fs regime, Phys. Rev. A **68**, 033806 (2003).

[23] M. Beijersbergen, R. Coerwinkel, M. Kristensen, and J. Woerdman, Helical-wavefront laser beams produced with a spiral phaseplate, Opt. Commun. **112**, 321 (1994).

[24] T. Roger, J. J. F. Heitz, E. M. Wright, and D. Faccio, Non-collinear interaction of photons with orbital angular momentum, Sci. Rep. **3**, 3491 (2013).

[25] A. Zaïr, M. Holler, A. Guandalini, F. Schapper, J. Biegert, L. Gallmann, U. Keller, A. S. Wyatt, A. Monmayrant, I. A. Walmsley, E. Cormier, T. Auguste, J. P. Caumes, and P. Salières, Quantum Path Interferences in High-Order Harmonic Generation, Phys. Rev. Lett. **100**, 143902 (2008).

[26] B. Mahieu, D. Gauthier, M. Perdrix, X. Ge, W. Boutu, F. Lepetit, F. Wang, B. Carré, T. Auguste, H. Merdji, D. Garzella, and O. Gobert, Spatial quality improvement of a ti:sapphire laser beam by modal filtering, Appl. Phys. B **118**, 47 (2015).

[27] K. Sueda, G. Miyaji, N. Miyanaga, and M. Nakatsuka, Laguerre-gaussian beam generated with a multilevel spiral phase plate for high intensity laser pulses, Opt. Express **12**, 3548 (2004).

[28] H. Ruf, Dynamique moléculaire par imagerie attoseconde, Ph.D. thesis, Bordeaux 1, 2012.

[29] E. Karimi and E. Santamato, Radial coherent and intelligent states of paraxial wave equation, Opt. Lett. **37**, 2484 (2012).

[30] F. Catoire, A. Ferré, O. Hort, A. Dubrouil, L. Quintard, D. Descamps, S. Petit, F. Burgy, E. Mével, Y. Mairesse, and E. Constant, Complex structure of spatially resolved high-order-harmonic spectra, Phys. Rev. A **94**, 063401 (2016).

[31] L. Rego, J. S. Román, A. Picón, L. Plaja, and C. Hernández-García, Nonperturbative Twist in the Generation of Extreme-Ultraviolet Vortex Beams, Phys. Rev. Lett. **117**, 163202 (2016).

[32] M. Ammosov, N. Delone, and V. Krainov, Tunnel ionization of complex atoms and of atomic ions in an alternating electromagnetic field, Sov. Phys. JETP **64**, 1191 (1986).

[33] C. Hernández-García, J. San Román, L. Plaja, and A. Picón, Quantum-path signatures in attosecond helical beams driven by optical vortices, New J. Phys. **17**, 093029 (2015).